Polarization studies in multiply scattering chiral media

I. Alex Vitkin
Department of Medical Biophysics
Ontario Cancer Institute/
University of Toronto
Toronto, ON, Canada M5G 2M9
E-mail: vitkin@oci.utoronto.ca

Emile Hoskinson
Department of Physics & Astronomy
University of British Columbia
Vancouver, BC, Canada V6T 1Z1
E-mail: hoskins@physics.ubc.ca

Abstract. The interactions of polarized light with an optically active (chiral), multiply scattering medium are investigated using a relatively simple experimental system incorporating polarization modulation and synchronous detection techniques. The polarization properties of diffusely scattered light are studied as a function of scatterer particle concentration, chiral molecule concentration, and detection direction. A newly derived method for simultaneous extraction of the total degree of polarization, and optical rotation of the linearly polarized fraction, is theoretically discussed and experimentally implemented, using optically thick turbid media with the presence of one chiral component. The method requires measurements at several orientations of the analyzing linear polarizer, followed by data fitting to yield the unknown sample polarization properties. The accuracy and robustness of this method in the cases of weak signals and noisy data are superior to previous two-point approaches of data analysis. The measurable polarization preservation on multiple scattering, affected by the chirality and turbidity of the medium and by the detection geometry as described, provides a useful tool with which to probe the properties of multiply scattering media. [S0091-3286(00)03602-3]

Subject terms: polarization; multiple scattering; chirality; polarimetry; phase modulation.

Paper 990242 received June 15, 1999; revised manuscript received Oct. 6, 1999; accepted for publication Oct. 14, 1999.

1 Introduction

There has been much research into the use of polarization data to characterize highly scattering turbid materials such as biological tissues, turbulent flows, and fog. This has resulted in recent discoveries of correlation and order-like effects in the light scattered from random heterogeneous media traditionally believed to completely ''scramble'' the polarization state, coherence, and direction of the incoming beam.[1–5] The fact that multiply scattered photons exhibit partial polarization preservation suggests a novel way to probe the characteristics of optically dense scattering media.[6,7]

In general, photons propagating in turbid media have their incident direction, phase, and polarization randomized by multiple scattering. The rate of depolarization depends on the initial polarization state, the number of scattering interactions, the efficiency and anisotropy of each scatter, and the properties of the ambient medium. The complexity of the heterogeneous system has not enabled the development of a general, complete, vector-wave multiple scattering theory, although various electromagnetic homogenization models may be applicable in some circumstances.[8,9] Many interesting and sometimes surprising effects due to the vector nature of light have recently been observed. For example, it has been noted that circularly polarized light preserves its polarization state better than linearly polarized light in a medium composed of anisotropic (forward-directed) Mie scatterers.[3,7] This type of scattering is particularly relevant in biomedical optics, as it applies to mammalian tissues in the red to near-IR part of the electromagnetic spectrum.[10] The opposite effect—better preservation of linear polarization—seems to hold in an isotropically Rayleigh-like scattering medium.[3,7] The influences of chirality of the turbid medium on these findings are beginning to be examined.[8,11,12]

Chirality (derived from the Greek word for ''hand'') is a property of materials, often biological in origin, that exhibit preferential handedness; that is, these materials have non-superimposable mirror images.[13] For example, glucose is such an asymmetric chiral molecule. As a result of this structural asymmetry, chiral substances interact differently with left and right circularly polarized light to manifest distinctive effects generically termed optical activity. The effects include, for example, circular dichroism and optical rotation, both of which are routinely used in transmission measurements to probe the subtle details of molecular structure and to determine the concentration of optically active chiral substances in largely transparent media[14] (e.g., a dilute protein suspension). However, these and other polarization techniques based on specular reflection are generally not suitable for detecting weak chiral asymmetries in optically heterogeneous thick turbid media. More sensitive methodologies are required for these systems to (1) detect the polarized fraction in the presence of a large depolarized background and (2) determine the effects of chirality on the measured signals, if any. Recently, these effects have been successfully observed in diffusive scattering from a two-phase turbid system,[11] whereby the presence of glucose molecules in the ambient fluid was found to enhance the

degree of polarization and optical rotation of scattered light.

In this paper, we investigate by means of birefringence modulation and synchronous detection the effects of the medium's chirality and turbidity, and the source-sample-detector geometry, on the polarization state of multiply scattered light. In Sec. 2, we derive the theoretical expressions pertaining to propagation of phase-modulated light in a multiply scattering chiral medium. A description of a simple experimental system based on polarization encoding via photoelastic phase modulation of incident light, and synchronous detection via lock-in amplification of scattered light, is given in Sec. 3. Several methods of data analysis are compared, with a detailed description of the most robust one that performs best in the low-signal, high-noise environment. Results of measurements from aqueous suspensions of polystyrene spheres containing varying amounts of glucose are presented in Sec. 4 to demonstrate the effects of chirality, turbidity, and viewing angle on the depolarization and optical rotation of the diffusely remitted light. Some implications of this study pertaining to noninvasive monitoring of glucose levels in biological systems using polarized light methodologies are also discussed.

2 Theory

The detection and analysis of light polarization in a turbid chiral medium in this study is based on a birefringence modulation device known as a photoelastic modulator[15] (PEM). Used with a synchronous detection scheme, this device enables sensitive measurements of a small polarized fraction in a predominantly depolarized background, as would be the case for diffusely scattered light. The operation and useful experimental arrangements for the PEM have been described elsewhere.[16,17] Briefly, it consists of a block of a transparent amorphous quartz driven into resonant oscillation at frequency f by a piezoelectric transducer, creating a time-dependent relative phase retardation between the components of the electric field transmitted parallel and perpendicular to its modulation axis.[17] In other words, for a suitably polarized incident beam, the light transmitted through the PEM exhibits a time-variable polarization state oscillating at a frequency f. The PEM is a particularly attractive instrument from an engineering design standpoint—its large aperture and wide acceptance angle imply relatively easy optical alignment; its wide useful spectral range (typically UV to mid-IR) make a single PEM suitable for measurements at many wavelengths; and its suitability for lock-in synchronous detection yields very narrow electronic bandwidths and thus high SNRs.

To derive useful expressions for optical activity of the chiral sample, and for the degree of polarization of multiply scattered light, consider the general experimental arrangement shown in Fig. 1. The effect of each optical component on the electric field of the transmitted beam is described by a standard 2×2 Jones matrix; the final result is evaluated by conventional matrix multiplication. While Jones calculus is preferred for its simplicity, it is best suited for treating fully polarized light; however, there are ways to account for depolarization effects.[12] In this paper, we introduce these explicitly [see discussion following Eq. (14)]. The alternative is to work with 4×4 Mueller (scattering) matrices and 4×1 Stokes vectors,[4,18–21] and such a detailed polarimetric description, while considerably more complex, may be appropriate for future studies. Working with x and y linear basis vectors convenient for describing the propagation of linearly polarized light through the system,* the Jones matrices for polarizers P1 and P2 are

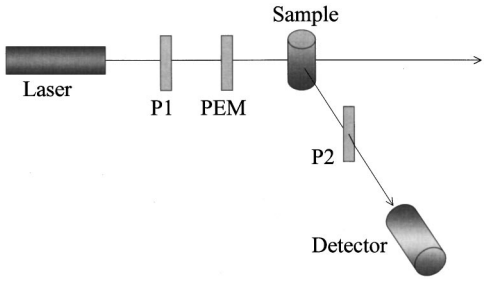

Fig. 1 General schematic of the optical polarization system for modeling polarized light interactions with a turbid chiral medium: P1 and P2, linear polarizers; PEM, photoelastic modulator.

$$\mathbf{P}i(@\,\theta_i)=\begin{bmatrix}\cos^2\theta_i & \cos\theta_i\cdot\sin\theta_i\\ \cos\theta_i\cdot\sin\theta_i & \sin^2\theta_i\end{bmatrix}, \tag{1}$$

where $\theta_{i=1,2}$ are the inclinations of the pass axes of the two polarizers with respect to the horizontal plane (θ=0 deg). The Jones matrix for the PEM, oriented at $\theta_{\mathrm{PEM}}=0$ deg without the loss of generality, is

$$\mathrm{PEM}(@0\ \mathrm{deg})=\begin{bmatrix}e^{i\delta} & 0\\ 0 & 1\end{bmatrix}, \tag{2}$$

where δ is the time-variable retardation of the PEM. It varies according to $\delta(t)=\delta_0\sin(2\pi ft)$, where δ_0 is the user-defined maximum retardation amplitude of the PEM element (e.g., $\lambda/4$ retardance), and f is the resonant frequency of oscillation ($\sim$50 kHz).

The sample matrix depends on its chiral properties. If the chiral sample exhibits circular dichroism A, defined as one half the difference between the absorptions of left and right circularly polarized light, $A=(A_L-A_R)/2$, its Jones description is

$$\begin{bmatrix}\cosh A & -\sinh A\\ \sinh A & \cosh A\end{bmatrix}. \tag{3}$$

If the sample is circularly birefringent, meaning that the real parts of its refractive index differ for left versus right circularly polarized light beams, this will manifest itself as an optical rotation of incident linearly polarized light. For sample rotation α, we have, in analogy with Eq. (3),

*It is also possible, and sometimes preferable, to work with **R** and **L** circular basis vectors, expressed in terms of the linear basis vectors as $\mathbf{R}=(x-iy)/\sqrt{2}$ and $\mathbf{L}=(x+iy)/\sqrt{2}$. The Jones matrices are modified to fit this description accordingly. For example, the optical rotation described by Eq. (4) becomes

$$\begin{bmatrix}\cos\alpha & -\sin\alpha\\ \sin\alpha & \cos\alpha\end{bmatrix}\cdot\begin{bmatrix}1\\1\end{bmatrix}\frac{E_0}{\sqrt{2}}\Big]_{x,y}\rightarrow\begin{bmatrix}e^{i\alpha} & 0\\ 0 & e^{-i\alpha}\end{bmatrix}\cdot\begin{bmatrix}1+i\\1-i\end{bmatrix}\frac{E_0}{2}\Big]_{R,L}.$$

$$\begin{bmatrix} \cos\alpha & -\sin\alpha \\ \sin\alpha & \cos\alpha \end{bmatrix}. \tag{4}$$

The sample also depolarizes the light; this important effect will be treated separately below. Prior to carrying out the matrix multiplication to determine the theoretical signal for the configuration represented in Fig. 1, two simplifications are possible. First, we neglect circular dichroism, since A was experimentally determined to be zero in all the samples examined in this study. Second, we can combine the effects of sample optical rotation [Eq. (4)] and polarizer orientation [Eq. (1)] into one matrix by simply redefining θ via $\theta=\theta\pm\alpha$ in Eq. (1), with $\pm$ accounting for both clockwise and counterclockwise senses of sample's optical rotation. If the sample is located between polarizer P1 and the PEM, then $\theta_1=\theta_1\pm\alpha$; when the sample is between the PEM and P2, $\theta_2=\theta_2\pm\alpha$. The latter arrangement was used exclusively for the results reported later in this paper. The matrix multiplication of the simplified product for the optical components shown in Fig. 1 then yields the electric field E impinging on the detector. Since the detector is polarization insensitive and measures light intensity, we find the latter through $I=E^*E$. After considerable algebraic manipulation and use of trigonometric identities, this gives

$$I\sim 2+\cos[2(\theta_1-\theta_2)]+\cos[2(\theta_1+\theta_2)] +\{\cos[2(\theta_1-\theta_2)]-\cos[2(\theta_1+\theta_2)]\}\cdot\cos[\delta(t)]. \tag{5}$$

Equation (5) contains an expression of the form $\cos[\delta]=\cos[\delta(t)]=\cos[\delta_0\cdot\sin(2\pi ft)]$. From a handbook of mathematical tables,[22] the following expansions are valid:

$$\cos[\delta_0\cdot\sin(\psi)]=J_0(\delta_0)+2\cdot J_2(\delta_0)\cdot\cos(2\psi)+\cdots$$

and

$$\sin[\delta_0\cdot\sin(\psi)]=2\cdot J_1(\delta_0)\cdot\sin(\psi)+2\cdot J_3(\delta_0)\cdot\sin(3\psi)+\cdots, \tag{6}$$

where $J_n(x)$ is the n'th-order Bessel function of x. These expansions will enable the decomposition of the detected signal into a dc component and ac components of different frequency harmonics.

We now examine two special cases pertinent to our study. In all our experiments, the sample was positioned between the PEM and the analyzer P2, and the PEM was always aligned in the horizontal plane ($\theta_{\mathrm{PEM}}=0$ deg). The first setup is the ''crossed-polarizer'' case (arrangement I), with $\theta_1=45$ deg and $\theta_2=-45$ deg$\pm\alpha$. From Eq. (5),

$$I_{\mathrm{I}}\sim 1-\cos(2\alpha)\cdot\cos(\delta), \tag{7}$$

which suggests that the detected signal can be used to measure the sample optical rotation α. Expanding the oscillatory term as a series of Bessel functions given in Eq. (6),

$$I_{(\mathrm{I})}\sim 1-\cos(2\alpha)J_0(\delta_0)-2\cos(2\alpha)J_2(\delta_0)\cos(2\omega t)-\cdots. \tag{8}$$

Taking the ratio of the signal components at $2f$ to that at dc yields

$$(2f/\mathrm{dc}_{\mathrm{I}})=\frac{-2J_2(\delta_0)\cos(2\alpha)}{1-J_0(\delta_0)\cos(2\alpha)}. \tag{9}$$

Note that there is a finite ac signal (at frequency $2f$) even if $\alpha=0$, as with an optically inactive sample or with no sample at all. The optical rotation can be determined from Eq. (9):

$$\cos(2\alpha)=\frac{(2f/\mathrm{dc})_{\mathrm{I}}}{-2J_2(\delta_0)+(2f/\mathrm{dc})_{\mathrm{I}}J_0(\delta_0)}. \tag{10}$$

The second special case of interest is obtained by rotating the second polarizer to the vertical position ($\theta_1=45$ deg, $\theta_2=90$ deg$\pm\alpha$), which yields

$$I_{(\mathrm{II})}\sim 1+\sin(2\alpha)\cos(\delta). \tag{11}$$

Performing the Bessel expansion from Eq. (6),

$$I_{(\mathrm{II})}\sim 1+\sin(2\alpha)J_0(\delta_0)+2\sin(2\alpha)J_2(\delta_0)\cos(2\omega t)+\cdots. \tag{12}$$

Thus,

$$(2f/\mathrm{dc})_{\mathrm{II}}=\frac{2J_2(\delta_0)\sin(2\alpha)}{1+J_0(\delta_0)\sin(2\alpha)}. \tag{13}$$

This arrangement also enables determination of the sample optical rotation α; from Eq. (13),

$$\sin(2\alpha)=\frac{(2f/\mathrm{dc})_{\mathrm{II}}}{2J_2(\delta_0)-(2f/\mathrm{dc})_{\mathrm{II}}J_0(\delta_0)}. \tag{14}$$

It is possible to experimentally set the maximum retardation to a value at which $J_0(\delta_0)$ vanishes. This simplifies the mathematics of signal analysis and yields good sensitivity for determining optical rotation. Alternatively, a good retardation setting is one that maximizes the $2f/\mathrm{dc}$ ratio; for example, for arrangement II and a realistic sample rotation α of several degrees or less, the optimum retardation setting of $\delta_0\sim 3.46$ rad follows from Eq. (13).

The preceding analysis assumes that the sample introduced only optical rotation, and did not depolarize the light. Now we must model the effects of multiple scattering as manifested in light depolarization. If the intensity of polarized light is p, and of unpolarized light due to sample scattering is u, we can define the degree of polarization as

$$\beta=\frac{p}{p+u}. \tag{15}$$

The unpolarized component contributes an additional dc signal. Carrying through the analysis for the polarized and the unpolarized components for arrangement I ($\theta_1=45$ deg, $\theta_2=-45$ deg$\pm\alpha$), there results, in analogy with Eq. (7),

$$I_{d(\mathrm{I})} \sim [1-\cos(2\alpha)\cos(\delta)]p+u. \tag{16}$$

Using the Bessel expansion from Eq. (6) and invoking Eq. (9), gives

$$(2f/\mathrm{dc})_{\mathrm{I}} = \frac{-2\beta J_2(\delta_0)\cos(2\alpha)}{1-\beta J_0(\delta_0)\cos(2\alpha)}. \tag{17}$$

This is the general modified version of Eq. (9) in the presence of a depolarized fraction produced by the turbidity of the medium. Similar analysis for arrangement II yields

$$(2f/\mathrm{dc})_{\mathrm{II}} = \frac{2\beta J_2(\delta_0)\sin(2\alpha)}{1+\beta J_0(\delta_0)\sin(2\alpha)}. \tag{18}$$

If the expected optical rotation α is small ($\sim$3 deg or less), we can replace $\cos(2\alpha)$ by unity, thus enabling direct determination of β from Eq. (17). Equation (18) then gives α. For the more general case of unrestricted rotation, we isolate the rotation angle α by combining Eqs. (17) and (18):

$$\tan(2\alpha) = \frac{[2J_2(\delta_0)/(2f/\mathrm{dc})_{\mathrm{I}}]+J_0(\delta_0)}{[2J_2(\delta_0)/(2f/\mathrm{dc})_{\mathrm{II}}]-J_0(\delta_0)}. \tag{19}$$

Once α is determined in this manner, the degree of polarization β can be calculated with the help of either Eq. (17) or Eq. (18). Thus, measurements at two angular orientations of P2 enable the extraction of both α and β. We will refer to this approach as the ratio method.

For a more accurate determination of these two important parameters, an alternate methodology was developed. Consider again Eq. (11), with P2 oriented at an angle of θ deg away from the vertical direction, P2 (at $90\pm\theta$ deg). In analogy with Eq. (18), the detected signal intensity in the presence of depolarizing scattering interactions will be

$$(2f/\mathrm{dc}) = \frac{2\beta J_2(\delta_0)\sin 2(\alpha+\theta)}{1+\beta J_0(\delta_0)\sin 2(\alpha+\theta)}. \tag{20}$$

Equation (20) is similar to Eq. (2b) of Ref. 11, except that the depolarization parameter β is now explicitly present; as such, this formalism suggests two more ways of determining α and β. The first way, designated the *2f* null method,[11] consists of adjusting the angular position of the P2 until the *2f* signal reaches a minimum (ideally approximately zero). The difference between this angle and the vertical is then equal to the sample optical rotation α. The degree of polarization β can be determined from Eq. (20) at any other known angle θ. Alternatively, measurements are made at several values of θ, obtained by turning P2 to different angular positions away from its nominal 90 deg orientation, followed by a nonlinear two-parameter fit in α and β, with θ as the independent variable (the fitting method). About 10 angular orientations of P2 were found to yield sufficient data set for a reasonable two-parameter fit to a given sample.

Both the ratio and the *2f* null methods require measurements at only two positions of P2 to determine α and β, and are thus relatively easy to perform; but given the sample variability and possible measurement artifacts as expected in future studies under realistic (nonlaboratory) conditions, their reliance on just two experimental points is perhaps disadvantageous. The fitting method entails more data collection, but is more robust and less prone to single-measurement mistakes. While we have verified the equivalence of the three methods for a given turbid chiral sample, and present some data below using all three approaches, the fitting method is our technique of choice for reproducible determination of α and β. In highly scattering samples and in certain detection directions where the polarization (*2f*) signals are weak, and the depolarized background large and noisy, the fitting method was the only one capable of furnishing reliable α and β results.

Finally, to quantify the scattering effects, we used Mie theory[23] to calculate the efficiency and angular dependence of light scattered by polystyrene spheres suspended in water and in glucose solutions. These two situations are different because dissolved glucose raises the refractive index n of water by $+0.025$/M,[24] reducing the refractive index mismatch between the spheres and the surrounding medium, and hence lowering their scattering strength. In addition, the scattering becomes more forward-peaked, as measured by the scattering anisotropy parameter g. For example, at a wavelength $\lambda=633$ nm, n(pure water)$=1.3315$, whereas $n(c_g=1.5$ M glucose$)=1.3690$. The refractive index of the spheres at 633 nm was calculated from the weighted average of their polymeric composition to be 1.575. The particle size distribution was measured with scanning electron microscopy to be nearly monodispersed spheres, with diameter $d=1.004\pm0.007$ μm. The Mie theory calculation yields the magnitude of the scattering efficiency Q and the scattering anisotropy g. For the range of glucose concentrations used in this study ($c_g=0$ to 1.5 M), the Q range was 2.38 to 1.83, close to the expected Mie result of $Q\sim2$ for objects larger than the wavelength. Note the significant variation in these results, caused by the refractive index matching due to dissolved glucose. The corresponding range in the scattering anisotropy g was 0.921 to 0.931. The volumetric scattering coefficient per unit length, μ, for a particular sample was determined from $\mu=QAN$, where $A=\pi(d^2/4)$ is the cross-sectional area of the microsphere, and N is their number per unit volume. For our samples with the scattering volume fraction $f_v=0$ to 0.2%, the scattering coefficient μ was typically $\lesssim40$ cm^{-1}. The corresponding mean free path is MFP$=1/\mu$, and the transport mean free path TMFP$=1/\mu(1-g)=1/\mu^*$, where $\mu^*=\mu(1-g)$ is the transport scattering coefficient. The optical thickness of the sample τ is calculated from $\tau=\mu t$, where $t=2.5$ cm is the diameter of the sample cuvette, with transport optical thickness $\tau^*=\tau(1-g)$.

3 Experimental Methods

Figure 2 shows a schematic of the polarization modulation and detection system used in this study. Light from a HeNe laser ($\lambda=632.8$ nm) passes through a linear polarizer P1 (45 deg) before impinging on the transparent fused quartz element of the photoelastic modulator (Hinds model PEM-80) with its modulation axis oriented horizontally (0 deg). The modulator element imparts a time-variable relative phase change $\delta(t)$ between the horizontal and vertical components of the passing beam at the resonant frequency of 50

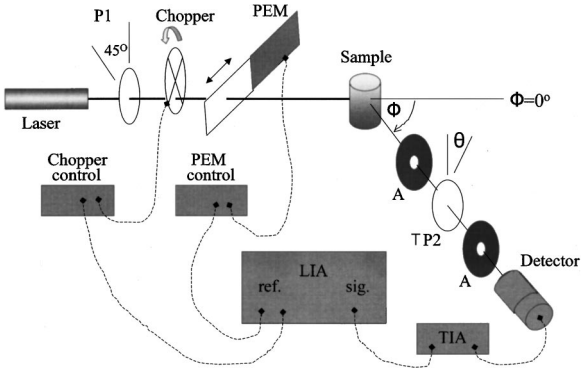

Fig. 2 Diagram of the apparatus for measuring the degree of polarization and optical rotation of scattered light. The detection angle Φ is defined with respect to the incident direction, and is varied by rotating the entire detector arm isocentrically about the sample cuvette: LIA, lock-in amplifier; TIA, transimpedance amplifier; A, apertures.

kHz, as described by $\delta(t)=\delta_0 \sin(2\pi ft)$. This causes the polarization of the exiting beam to vary in a predictable and periodic fashion. The extreme states between which the polarization varies are determined by the magnitude of the maximum PEM retardation δ_0. The light is then scattered by the turbid chiral sample, passes through an analyzer P2 (oriented at angle θ), and is detected by an end-window photomultiplier tube. The photocurrent passes through a preamp and is registered by a lock-in amplifier synchronized by the PEM driver, thus enabling detection of the signal components at modulation frequencies *f* or *2f*. The overall light intensity (essentially the dc component of the photocurrent) is monitored by mechanically chopping the light issuing from the HeNe laser at a low frequency of ~77 Hz, and using the same lock-in amplifier for synchronous detection. Pinhole diaphragms are used as apertures *A* for reduction of stray light and for better definition of incident and detection angles. The resultant acceptance angle of the detector was a 15 mrad (2.2×10^{-4} sr) cone set on the sample center. To enable signal measurement as a function of angle Φ, the liquid sample was poured into a cylindrical cuvette placed at the pivot of an isocentrically rotating arm containing the detection elements. Thus, both the incident and detected light were normal to the cylindrical cuvette glass wall that contains the turbid suspensions (cuvette inner diameter=2.50 cm, volume~25 ml). All reported measurements were conducted at room temperature.

Several experimental caveats discovered in the process of this study deserve special mention. First, the PEM was rotated in the horizontal plane by about 8 to 10 deg to reduce significant interference effects observed at normal incidence due to internal reflections.[25] Although antireflection coating is an effective alternative solution for the single-wavelength measurements described here, the wideband advantage of the PEM technology for other experiments would be sacrificed. Second, a maximum of 2 h after dissolving glucose in water was needed prior to experiments, to allow sufficient time for the optical rotatory power of the solutions to stabilize. This effect is known as metarotation;[26] we found a ~60% reduction in the measured rotation from a maximum just after mixing to stabilization after about 2 h.

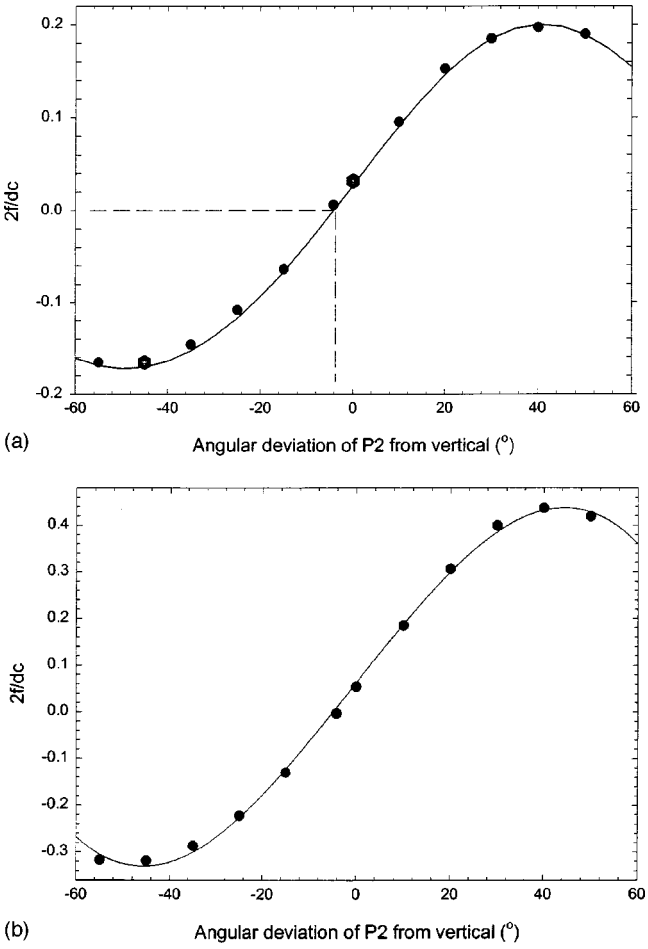

Fig. 3 (a) Variation in the $2f$/dc values with angular orientation of P2, for a turbid chiral sample with $c_g=1.5$ M, and $f_v=0.1\%$ ($Q=1.83$, $g=0.931$, $\mu=27.3$ cm^{-1}, MFP=0.36 mm, TMFP=5.31 mm, $\tau=68$). The detection was done in the lateral direction at $\Phi=90$ deg. The maximum PEM retardation amplitude was $\delta_0=3.462$ rad. This value was chosen to maximize Eq. (20) for expected optical rotations ($\alpha\lesssim10$ deg), hence optimizing weak signal detection. Negative ordinate values correspond to negative phase readings on the lock-in amplifier. The data points are the experimental values; the solid line is the result of the fitting method with optimized values of α and β from Eq. (20); the dashed lines show the determination of α from the *2f* null method, with β then determined from the central hexagon data point via Eq. (18); and the two hexagon data points correspond to arrangements I and II of the ratio method, with α and β deduced from Eqs. (17) and (19). The results for (α,β) are (4.4 $\pm$0.2 deg, 19.1$\pm$0.5%)$_{\text{fitting}}$; (4.2 deg, 18%)$_{2f\ \text{null}}$; (4.1 deg, 19%)$_{\text{ratio}}$. (b) Results and fitting method analysis from a similar experiment as above, except with a weaker scattering sample of $f_v=0.07\%$. The results for (α,β) are (3.8$\pm$0.2 deg, 40.0$\pm$0.8%)$_{\text{fitting}}$; (3.6 deg, 37%)$_{2f\ \text{null}}$; (3.7 deg, 41%)$_{\text{ratio}}$. As shown, the fitting method was judged to be the most robust for extraction of α and β from PEM measurements, and was used for all the subsequent data analysis presented in the paper.

4 Results and Discussion

Figure 3(a) shows a comparison of the three methods for determining α and β. For this experiment, the detection was done laterally at $\Phi=90$ deg, a detection direction that may be suitable in potential materials analysis or biomedical diagnostic applications. The data points are the $2f$/dc values versus P2 angular orientation for a 1.5-M glucose

sample with 1.0 g/l polystyrene microsphere concentration. The solid line is from the fitting method with Eq. (20), with optimized α and β as the fitting parameters. The standard deviations in the fitted values were $\Delta\alpha = \pm 5\%$ and $\Delta\beta = \pm 2\%$; these uncertainties were typical of the performance of the fitting method in a variety of turbid samples. The dotted lines mark the location of the *2f* null signal, indicating α directly; β is then obtained from a measurement with P2 vertical and Eq. (18). The hexagon points are 45 and 90 deg measurements corresponding to arrangements I and II needed for the ratio method, which yield α from Eq. (19) and β from Eq. (14). The resultant α and β determined by each method are given in the figure caption. The uncertainties are given only for the fitting method, as the other two-point approaches are not easily amenable to direct estimate of errors. The agreement in optical rotation values between the three methods is reasonable for this sample, as is the agreement in degree of polarization between the ratio and the fitting methods. Another representative result for a sample with lower polystyrene concentration of 0.7 g/l, analyzed with the fitting method, is shown in Fig. 3(b). Note the increase in the $2f/\mathrm{dc}$ values for this lower scattering sample (at least for $\Phi = 90$ deg). As these and other data sets illustrate, the observed optical activity and depolarization effects in multiple scattering are well modeled by the developed theory. Also note that while one might expect that α depends only on chirality and β depends only on turbidity, the actual situation is more complicated—in this case, the decrease in the scattering coefficient likely causes a decrease in the effective pathlength traversed by the detected light, yielding smaller optical rotation and larger polarization preservation.

Figure 4(a) shows optical rotation α as a function of the detection angle Φ. The data are for a 1.5-M glucose sample with a polystyrene microsphere concentration of 1.3 g/l. The rotation displayed in Fig. 4(a) can be translated into an equivalent pathlength $\langle L \rangle$ from $\langle L \rangle = \alpha/(c_g R)$, since we know the specific optical rotatory power R of glucose at this wavelength and temperature. Using manufacturer's data (independently verified in clear glucose solutions), $R = 4.8$ deg cm^2 g^{-1}, we arrive at the pathlength scale represented on the right-hand ordinate of the graph. The arrow at 2.5 cm represents the diameter of the sample cuvette.

Figure 4(a) includes several interesting features. The average pathlength traveled by the light through the sample can be both larger and smaller than the cuvette diameter. For small detection angles in the forward direction, multiple scattering increases the effective pathlength of the light. For larger detection angles, the pathlength decreases; evidently, the light detected at these angles has not penetrated as far into the cell interior, or has not scattered back out as effectively in reaching the detector while preserving the optical rotation information. Note that only light that remains polarized contributes to the measured rotation via the *2f* signal component, and thus to the deduced pathlength. Light that becomes entirely depolarized may well experience a different, larger pathlength, or conversely, a longer pathlength is likely to cause greater depolarization. It is also possible that there is rotation reversal (''helicity flip''[2]) occurring, as with light that traverses back and forth through a transparent chiral medium, causing the detected rotation to decrease; thus, although the actual pathlength

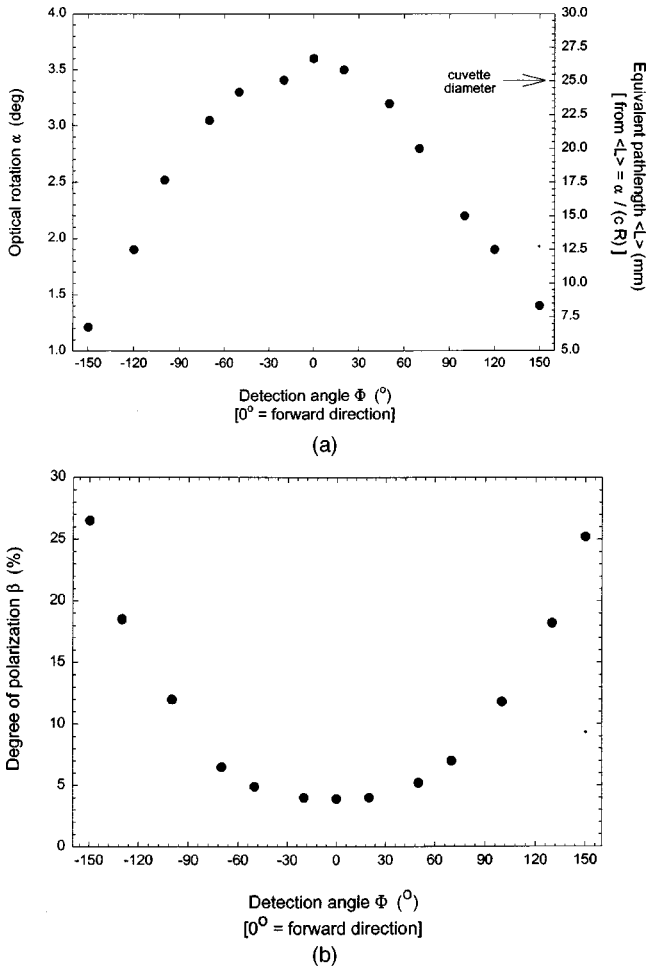

Fig. 4 Polarization analysis of light scattered from a turbid chiral sample with $c_g = 1.5$ M and $f_v = 0.13\%$ ($Q_{sc} = 1.83$, $g = 0.931$, $\mu = 35.5$ cm^{-1}, MFP = 0.28 mm, TMFP = 4.1 mm, $\tau = 89$), as a function of detection angle Φ. At each Φ direction, measurements of the $2f/\mathrm{dc}$ ratios were taken at nine different angular orientations of the polarizer P2 to ensure sufficient data for an accurate and robust performance of the fitting method. The plots display the deduced (a) optical rotation and (b) degree of polarization.

may be large, the effective pathlength as derived from accumulated rotation appears smaller. This helicity reversal, manifest as an optical rotation of opposite sense, has been suggested and detected previously in the near-back-scattering direction.[2,11] Note also that the signal is symmetrical about the forward direction ($\Phi = 0$ deg). We are currently modifying our experimental setup to enable more measurements in the backwards direction beyond $\Phi = \pm 150$ deg, and specifically at $\Phi = 180$ deg to examine further the back-scattering polarization signals.

Figure 4(b) shows the degree of polarization β from the same sample. The systematic variation of β with angle shows the opposite trend of that of optical rotation or pathlength, and the data is once again symmetric about the forward direction. The longer the pathlength (larger α, forward directions), the more the multiple scattering process depolarizes the light. Similarly, in lateral and back directions (smaller α's for this sample), the shorter pathlengths result in higher polarization preservation. This inverse correlation between pathlength and degree of polarization

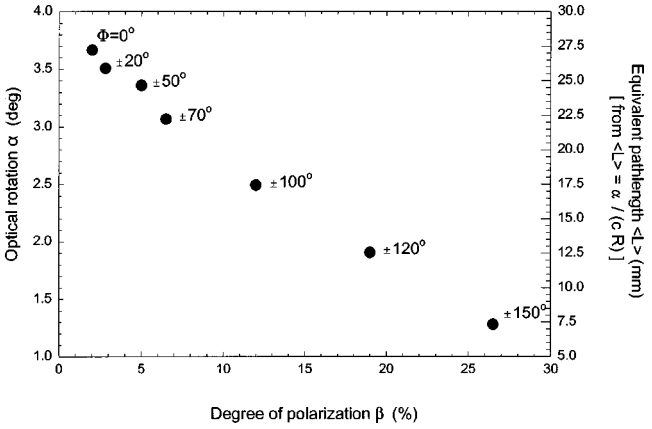

Fig. 5 Relationship between average pathlength $\langle L \rangle$ and degree of polarization β, obtained from the data of Figs. 4(a) and 4(b). The detection angles at which the measurements were made to determine each $(\langle L \rangle, \beta)$ pair are indicated beside the data points.

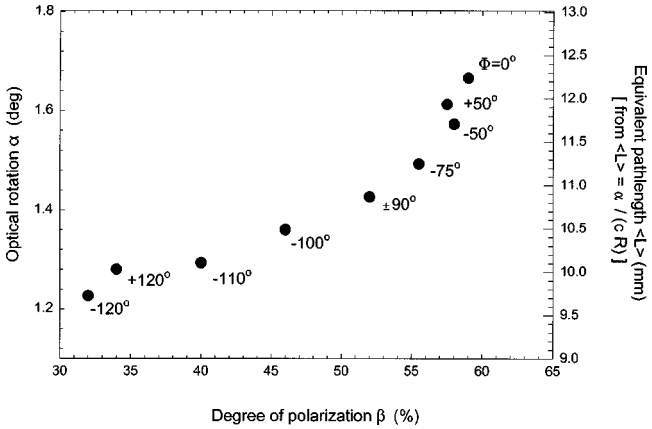

Fig. 6 Relationship between average pathlength $\langle L \rangle$ and degree of polarization β, at different detection angles for a turbid chiral sample with $c_g = 1.0$ M and $f_v = 0.04\%$ ($Q = 2.01$, $g = 0.928$, $\mu = 12.3$ cm^{-1}, MFP = 0.81 mm, TMFP = 11.3 mm, $\tau = 31$). See captions to Figs. 4 and 5 for more details.

seems reasonable, implying that whether or not there is helicity reversal at large detection angles, more extensive scattering depolarizes the light but engenders a greater effective rotation to the surviving polarized fraction.

The relationship between pathlength and degree of polarization is further analyzed in Fig. 5. The data looks strikingly linear over the whole range of detection angles. This suggests that the knowledge of β may be used to predict $\langle L \rangle$; then, with the α data obtained from the same PEM measurement, the concentration of glucose c_g can be obtained from $c_g = \alpha / (\langle L \rangle R)$. While this is routinely done in transparent dilute solutions where the optical path $\langle L \rangle$ is well known, the determination of the concentration of chiral species in a multiply scattering system would be very exciting. It is important to note that the linear dependence of β on $\langle L \rangle$ seen in this example is not imperative, and other relationships are useful as long as the functional dependence between β and $\langle L \rangle$ can be deduced. Even determination of pathlength $\langle L \rangle$ alone, without specifying c_g, would be a very important step in understanding the propagation of light, and polarization interactions, in multiply scattering media.[5] The potential of this approach in more complicated scattering media containing multiple chiral species, for example in biological tissues, is currently under examination in our laboratory.

The variation of α and β with the detection angle is influenced by the optical properties of the material. Figure 6 shows the results from a 1-M glucose, 0.41 g/l polystyrene microsphere concentration sample. The data for this sample seems to show more scatter as a function of Φ, and is less symmetric about the forward direction. Whereas the optical rotation dependence is similar to Fig. 4(a), the dependence of the degree of polarization on detection angle is opposite of Fig. 4(b)—the forward-directed photons best maintain their polarization. Thus, the plot of pathlength versus β now shows a direct relationship, in contrast with the inverse dependence of Fig. 5. It may be that the helicity-reversal mechanism discussed earlier is more important for this sample, and the simple determination of pathlength from optical rotation may be in error [right ordinate of Fig. 4(a)]. As well, the dependence of the degree of polarization on pathlength may be more complicated—the actual shape of $\langle L \rangle$ as well as its magnitude may be important. For example, a tortuous zigzag path with many small-angle deflections, and a more jagged path with several large-angle scattering events will likely depolarize the light to different extent, even though the magnitude of $\langle L \rangle$ may be equal for both parts.

The effects of varying the sample turbidity on the depolarization of laterally scattered light are shown in Fig. 7(a). The results are for two sets of turbid suspensions spanning the same microsphere concentration range (~0.1 to 1.5 g/l), with the top curve for 1.5-M glucose samples, and bottom curve for glucose-free samples. The decrease of β with f_v is clearly seen for both sets of suspensions, although the β values are higher, and their rate of decrease slower, in the chiral set. This was noted previously[11,12] in the backscattering direction ($\Phi \sim 174$ deg) in a similar experimental system, with a convincing heuristic explanation for, and quantification of, the polarization-preserving effect of glucose. The explanation invokes the preferential polarization retention of circularly polarized light in a medium with predominantly forward scatterers,[2,4] and a glucose effect that causes propagating light waves to assume just that polarization state.[8] One must, however, examine the direct influence of glucose-induced refractive index-matching on reduction of scattering intensity, and increase in scattering anisotropy, to determine if these alone account for observed enhancement of polarization preservation. After the necessary Mie scattering calculations, Fig. 7(b) shows the same data replotted against the common scattering coefficient μ; in Fig. 7(c), the common abscissa axis is now the transport scattering coefficient μ^*. As seen, progressing from a common microsphere concentration to a common scattering coefficient to a common reduced scattering coefficient reduces the differences in polarization preservation in the presence and absence of glucose; however, the difference in the data remains clearly visible. Thus, it appears that refractive index-matching is not the only reason for enhanced polarization preservation in these turbid glucose solutions. This is in contrast to previously published data,[11,12]

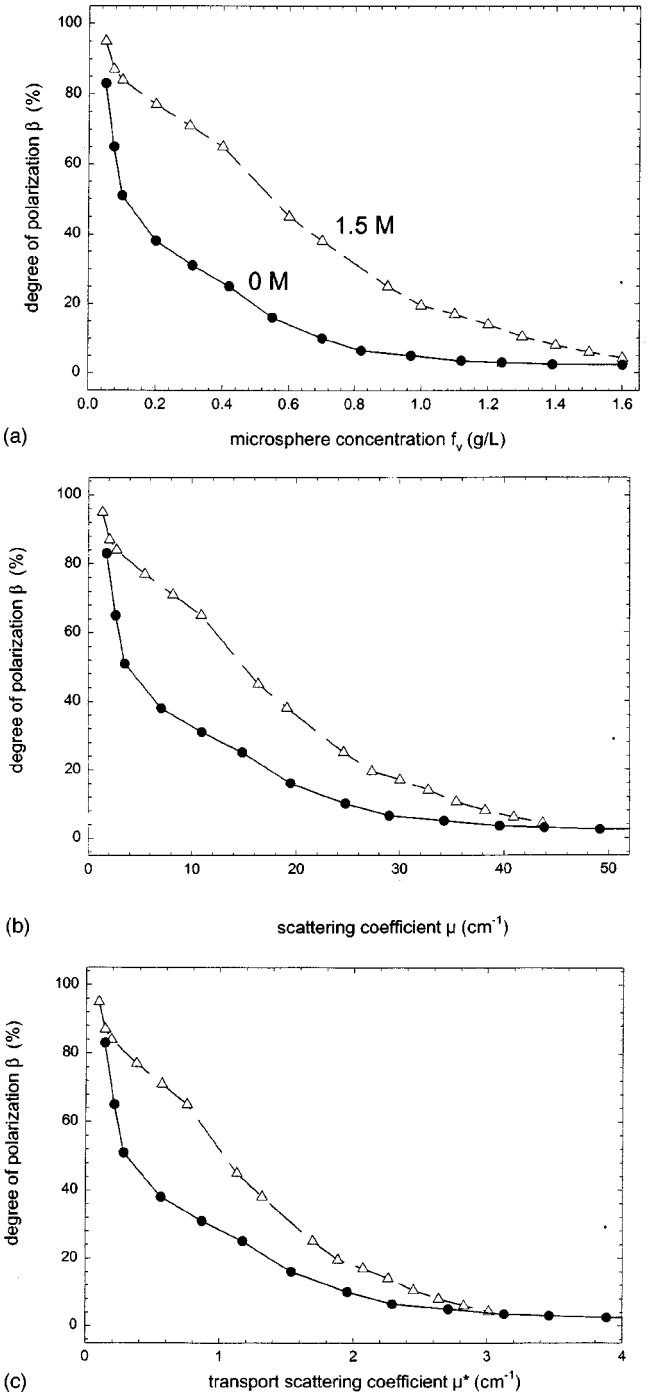

Fig. 7 Depolarization of laterally scattered light as a function of sample turbidity, with and without the presence of glucose. The abscissa axis in units of (a) microsphere concentration f_v, (b) scattering coefficient μ, and (c) transport scattering coefficient $\mu^* = \mu(1 - g)$. These transformations are necessary to account for the refractive index matching effect of dissolved glucose.

where, despite the higher glucose concentration of ~2.8 M, the β behavior becomes similar in chiral and achiral scattering samples once the preceding analysis of refractive index matching is performed. Different experimental conditions—detection angle, light wavelength, sample holder, methods of data analysis—are likely responsible for this observed difference.

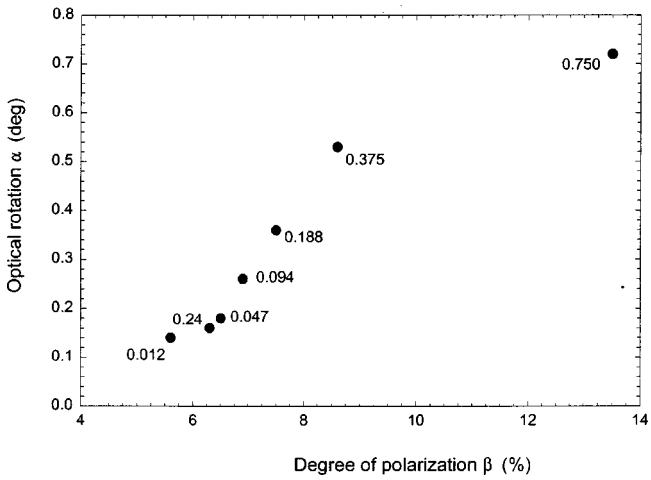

Fig. 8 Variation in optical rotation α degree of polarization β with glucose concentration, detected in the lateral direction for samples with a fixed microsphere concentration $f_v = 0.10\%$. For zero glucose concentration, this yields the following scattering properties: $Q = 2.37$, $\mu = 35.6\ cm^{-1}$, $g = 0.921$, MFP = 0.28 mm, TMFP = 3.56 mm, and $\tau = 89$. At the highest glucose concentration (135 g/l = 0.75 M), the refractive index-matching effect changes the scattering parameters to $Q = 2.09$, $g = 0.927$, $\mu = 31.4\ cm^{-1}$, MFP = 0.32 mm, TMFP = 4.38 mm, and $\tau = 79$. The glucose concentration (in molar units) at which the measurements were made to determining each (α,β) pair are indicated beside the data points.

The dependence of optical rotation and degree of polarization on the chiral content of the material (0.012 to 0.750 M glucose) is further examined in Fig. 8 in a sample set with a fixed amount of scattering microspheres (1 g/l) and lateral detection direction. The results are presented in a parametric plot similar to those in Figs. 5 and 6, except here the glucose concentration and not the detection angle acts as the independent variable. As expected, the angle of rotation increases with glucose concentration; in addition, polarization preservation is higher. In analogy with the analysis of Fig. 7, note that despite constant microsphere concentration, these samples do not have the same scattering properties, due to dissolved glucose. Thus, some enhancement in polarization preservation can be expected simply because of decreasing scattering. As detailed in the figure caption, there is a ~12% reduction in the scattering coefficient and a ~19% reduction in transport scattering coefficient over this glucose concentration range. Can these modest scattering changes alone cause the observed ~100% increase in β? Further modeling studies will address this question, but qualitatively it appears unlikely that the refractive index-matching mechanism is the sole cause of diminished depolarization. As mentioned, another possible reason is that the optical eigenmodes in a chiral medium correspond to circularly polarized light, which is better preserved in an anisotropically scattering system, as is the case for the present experiments. Precise explanation notwithstanding, the observed trend is important: for approximately constant scattering, higher α and β may indicate the presence of a chiral species.

Based on the presented results and the additional measurements of reproducibility and accuracy not reported here, we estimated the following operating characteristics of our present experimental system, with data analysis us-

ing the fitting method. As tested, the uncertainty in the degree of polarization determination is $\Delta\beta = \pm 2\%$, while that in optical rotation is $\Delta\alpha = \pm 5\%$. For the optically thick suspension examined in this paper, the low detection limit of dissolved glucose in multiply scattering samples is approximately 0.010 M, although this value is significantly effected by the actual turbidity and detection geometry of a particular experiment. We are currently examining experimental refinements capable of extending the lower limit of glucose detectivity and accuracy (via *both* α and β determination) in highly scattering media.

5 Summary and Conclusions

One would think that polarized light launched into a multiply scattering medium would escape completely depolarized. This, however, is not so—depending on the optical and geometric properties of the sample, the initial polarization state, and source-detection geometry, the scattered light may exhibit a significant surviving polarization fraction. We have used a polarization-modulation and synchronous detection technique to quantify the surviving polarization properties of light multiply scattered in different directions from turbid chiral samples. The two parameters derivable from our experiments are the net degree of polarization and the optical rotation of linearly polarized light. A robust method for their derivation, applicable to weak signal measurements in a noisy background, was described and tested. As tested, our percentage accuracy in the degree of polarization determination is typically $\Delta\beta = \pm 2\%$, while that in optical rotation is $\Delta\alpha = \pm 5\%$. For the optically thick suspension examined in this study, the lower detection limit of dissolved glucose in diffusive scattering is approximately 0.010 M. The actual value is dependent on the type of scattering interactions and the magnitude of the scattering coefficients, and will likely be different (probably higher) in, for example, optically thick biological tissues.

The observed dependencies of α and β on the sample scattering properties, chiral properties, and measurement geometry, suggest promising experimental strategies for further scientific and technological developments of the presented methodology. For example, earlier work[2,4] suggests that in the retroreflection direction ($\Phi \sim 180$ deg) from a turbid medium comprised of Mie-like scatterers, the degree of polarization for incident circularly polarized light remains finite for very large values of optical thickness. This information channel may thus be available to examine the properties of turbid media, including those with large scattering coefficients. We are currently examining the effect of chirality on this polarization memory of circularly polarized light, using the PEM methods outlined in this paper.

While the described relatively simple methodology is well suited for the model samples examined in this paper, much research remains in applying it to more complex systems, for example, biological tissues for the purpose of optical imaging[7] (also see, e.g., Ref. 27), thermal damage assessment,[28] or noninvasive glucose monitoring (see, e.g., Ref. 29). First, as presented, the sensitivity of the measurement must be considerably improved for potential noninvasive glucose monitoring. Measurements at several wavelengths, and determination of other chiral asymmetries in the polarization signature of scattered light, are being investigated. Also, considerably more complex experimental methods, such as the use of several PEMs,[19] closed-loop feedback control,[30] and optical interferometry,[31] are being evaluated for their suitability to polarization studies in optically thick heterogeneous media. It is important to note that although some of these methods achieve millidegree sensitivity in optical rotation, they are primarily optimized for transparent or dilute solutions, and do not furnish the measure of depolarization. The presented methodology, while presently lacking optical rotation sensitivity of the just-mentioned methods, offers relative simplicity of data collection and analysis, is well suited for diffusive polarization measurements from optically dense samples, and yields two important polarization characteristics, namely, α and β. We are also addressing the fundamental issue of whether the polarization effects reported here in a discrete scattering media are also seen if the nature of the scattering medium is different. For example, biological tissues belong to a class of scattering systems loosely termed ''random continua,''[32] and it is likely that the details of their interaction with polarized light are altered. The native optical birefringence of many biological tissues must also be accounted for. Work is in progress to quantify polarization effects in these types of turbid systems for potential applications in remote sensing, materials characterization, and biomedical diagnostics.

Acknowledgments

This work was supported by a grant from the Natural Sciences and Engineering Research Council of Canada.

References

1. P. E. Wolf and G. Maret, ''Weak localization and coherent backscattering of photons in disordered media,'' *Phys. Rev. Lett.* **55**, 2696–2699 (1985).
2. F. C. MacKintosh, J. X. Zhu, D. J. Pine, and D. A. Weitz, ''Polarization memory of multiply scattered light,'' *Phys. Rev. B* **40**, 9342–9345 (1989).
3. R. Berkovits and M. Kaveh, ''The vector memory effects for waves,'' *Europhys. Lett.* **13**, 97–101 (1990).
4. A. S. Martinez and R. Maynard, ''Polarization statistics in multiple scattering of light: a Monte Carlo approach,'' in *Photonic Band Gaps and Localization*, C. M. Souloukis, Ed., pp. 99–114, Plenum Press, New York (1993).
5. M. Dogariu and T. Asakura, ''Photon pathlength distribution from polarized backscattering in random media,'' *Opt. Eng.* **35**, 2234–2239 (1996).
6. J. M. Schmitt, A. H. Gandjbakhche, and R. F. Bonner, ''Use of polarized light to discriminate short path photons in a multiply scattering medium,'' *Appl. Opt.* **31**, 6535–6546 (1992).
7. S. L. Jacques, M. Ostermeyer, L. Wang, and D. Stephens, ''Polarized light transmission through skin using video reflectometry: toward optical tomography of superficial tissue layers,'' *Proc. SPIE* **2671**, 199–210 (1996).
8. A. Lakhtakia, *Beltrami Fields in Chiral Media*, Chap. 9, World Scientific Publishing, Singapore (1994).
9. B. Michel and A. Lakhtakia, ''Strong property fluctuation theory for homogenizing chiral particulate composites,'' *Phys. Rev. E* **51**, 5701–5707 (1995).
10. W.-F. Cheung, S. A. Prahl, and A. J. Welch, ''A review of optical properties of biological tissues,'' *IEEE J. Quantum Electron.* **26**, 2166–2185 (1990).
11. M. P. Silverman, W. Strange, J. Badoz, and I. A. Vitkin, ''Enhanced optical rotation and diminished depolarization in diffusive scattering from a chiral liquid,'' *Opt. Commun.* **132**, 410–416 (1996).
12. M. P. Silverman, *Waves and Grains*, Chap. 13, Princeton University Press, Princeton, NJ (1997).
13. J. Applequist, ''Optical activity: Biot's bequest,'' *Am. Sci.* **75**, 59–67 (1987).
14. L. D. Barron, *Molecular Light Scattering and Optical Activity*, Cambridge Press, London (1982).
15. J. C. Kemp, ''Piezo-optical birefringence modulators: new use for a long-known effect,'' *J. Opt. Soc. Am.* **59**, 950–954 (1969).

16. J. Badoz, M. Billardon, J. C. Canit, and M. F. Russel, ''Sensitive devices to measure the state and degree of polarization of a light beam using a birefringence modulator,'' *J. Opt. (Paris)* **8**, 373–384 (1977).
17. M. P. Silverman, N. Ritchie, G. M. Cushman, and B. Fisher, ''Experimental configurations using optical phase modulation to measure chiral asymmetries in light specularly reflected from a naturally gyroptopic medium,'' *J. Opt. Soc. Am. A* **5**, 1852–1863 (1988).
18. A. J. Hunt and D. R. Huffman, ''A new polarization-modulated light scattering instrument,'' *Rev. Sci. Instrum.* **44**, 1753–1762 (1973).
19. R. C. Thompson, J. R. Bottiger, and E. S. Fry, ''Measurement of polarized light interactions via the Mueller matrix,'' *Appl. Opt.* **19**, 1323–1332 (1980).
20. B. D. Cameron, M. J. Rakovic, M. Mehrubeouglu, G. Kattawar, S. Rastegar, L. V. Wang, and G. L. Cote, ''Measurement and calculation of the two-dimensional backscattering Mueller matrix of a turbid medium,'' *Opt. Lett.* **23**, 485–487 (1998).
21. A. H. Hielscher, A. A. Eick, J. R. Mourant, J. P. Freyer, and I. J. Bigio, ''Biomedical diagnostic with diffusely backscattered linearly and circularly polarized light,'' *Proc. SPIE* **2976**, 298–305 (1997).
22. M. Abramowitz and I. A. Stegun, *Handbook of Mathematical Functions*, p. 361, Dover, New York, NY (1965).
23. C. F. Bohren and D. R. Huffman, *Absorption and Scattering of Light by Small Particles*, Appendix A, Wiley Interscience, New York (1983).
24. R. C. Weast, Ed., *Handbook of Chemistry and Physics*, Chemical Rubber Company, Cleveland, OH (1973).
25. T. C. Oakberg, ''Modulated interference effects: use of photoelastic modulators with lasers,'' *Opt. Eng.* **34**, 1545–1550 (1995).
26. T. M. Lowry, *Optical Rotatory Power*, Longmans and Green, Washington, DC (1935).
27. *Diffusing Photons in Turbid Media*, a feature issue of *Appl. Opt.* **36**, 9–231 (1997).
28. V. Sankaran and J. T. Walsh, ''Birefringence measurement of rapid structural changes during collagen denaturation,'' *Photochem. Photobiol.* **68**, 846–851 (1998).
29. T. W. King, G. L. Cote, R. McNickols, and M. J. Goetz, ''Multispectral polarimetric glucose detection using a single Pockels cell,'' *Opt. Eng.* **33**, 2746–2753 (1994); J. Qu and B. C. Wilson, ''Monte Carlo modeling studies of the effect of physiological factors and other analytes on the determination of glucose concentration *in vivo* by near infrared optical absorption and scattering measurements,'' *J. Biomed. Opt.* **2**, 319–325 (1997), and references contained therein.
30. B. D. Cameron and G. L. Cote, ''Noninvasive glucose sensing utilizing a digital closed-loop polarimetric approach,'' *IEEE Trans. Biomed. Eng.* **44**, 1221–1227 (1997).
31. C. Chou, Y.-C. Huang, C.-M. Feng, and M. Chang, ''Amplitude sensitive optical heterodyne and phase lock-in technique on small optical rotation angle detection of chiral fluid,'' *Jpn. J. Appl. Phys.* **36**, 356–359 (1997).
32. A. Ishimaru, *Wave Propagation and Scattering in Random Media*, Academic Press, New York (1978); A. J. Welch and M. J. C. van Gemert, Eds., *Optical-Thermal Effects in Laser-Irradiated Tissue*, Chap. 2, Plenum Press, New York (1995).

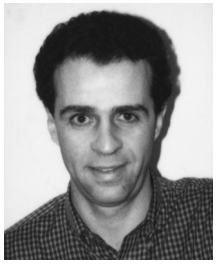

I. Alex Vitkin received his BASc from Queen University, Kingston, Canada, in 1985, his MASc in mechanical engineering from University of Toronto, Canada, in 1989, and his PhD in medical physics from McMaster University, Hamilton, Canada, in 1994. He is currently an assistant professor in the Departments of Medical Biophysics and Radiation Oncology at the University of Toronto, a clinical physicist at the Princess Margaret Hospital, and an associate scientist at the Ontario Cancer Institute. His research interests are in biophotonics, and include photothermal effects in tissues, polarized light propagation in turbid media, and optical coherence tomography.

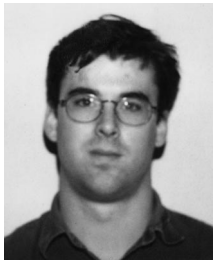

Emile Hoskinson received his BSc from the University of British Columbia, Vancouver, Canada, in 1999. He is currently a PhD candidate with the Department of Physics at the University of California, Berkeley. His areas of interests include optical and acoustic scattering and localization, high temperature superconductivity, and superfluid weak links.